analytical chemistry

Article

pubs.acs.org/ac

# Measurement of Small Molecule Binding Kinetics on a Protein Microarray by Plasmonic-Based Electrochemical Impedance Imaging

Wenbin Liang,[†,‡] Shaopeng Wang,*[,†] Fernanda Festa,[§] Peter Wiktor,[†] Wei Wang,[†,⊥] Mitchell Magee,[§] Joshua LaBaer,*[,§] and Nongjian Tao*[,†,∥]

[†]Center for Bioelectronics and Biosensors and [§]Center for Personalized Medicine, Biodesign Institute, Arizona State University, Tempe, Arizona 85287, United States

[‡]Department of Clinical Biochemistry, Laboratory Sciences, Third Military Medical University, 30 Gaotanyan Street, Shapingba District, Chongqing 400038, China

[∥]Department of Electrical Engineering, Arizona State University, Tempe, Arizona 85287, United States

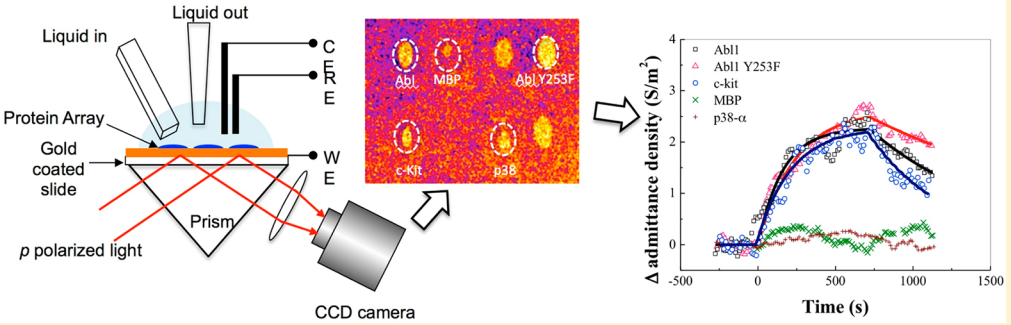


**ABSTRACT:** We report on a quantitative study of small molecule binding kinetics on protein microarrays with plasmonic-based electrochemical impedance microscopy (P-EIM). P-EIM measures electrical impedance optically with high spatial resolution by converting a surface charge change to a surface plasmon resonance (SPR) image intensity change, and the signal is not scaled to the mass of the analyte. Using P-EIM, we measured binding kinetics and affinity between small molecule drugs (imatinib and SB202190) and their target proteins (kinases Abl1 and p38-$\alpha$). The measured affinity values are consistent with reported values measured by an indirect competitive binding assay. We also found that SB202190 has weak bindings to ABL1 with $K_D$ > 10 $\mu$M, which is not reported in the literature. Furthermore, we found that P-EIM is less prone to nonspecific binding, a long-standing issue in SPR. Our results show that P-EIM is a novel method for high-throughput measurement of small molecule binding kinetics and affinity, which is critical to the understanding of small molecules in biological systems and discovery of small molecule drugs.

Proteins act by interacting with other proteins and biomolecules. Important biological processes, such as communications between cells, expression of genes, and immune response, rely on specific interactions between proteins and other molecules, including small molecules. Studying protein interactions is critical to the discovery of biomarkers for disease diagnosis, and drugs for disease treatment. Protein interactions are quantified by binding kinetic constants and affinities, and determining these parameters is thus a basic task in studying and quantifying protein interactions.

Current methods for measuring protein interactions fall into two categories: label- and label-free-based methods. Label-based methods, such as fluorescence detection, are mostly end-point assays that do not provide kinetics information. Furthermore, the use of dye molecules in fluorescence detection can significantly alter the native properties of proteins, leading to inaccurate conclusions.[1] Label-free methods, such as surface plasmon resonance (SPR),[2−8] can provide kinetics information, but they often suffer from interference caused by nonspecific bindings and bulk index changes.[9] In addition, the SPR signal is proportional to the mass of the molecule, so its sensitivity diminishes with the size of the molecule, making it extremely challenging to detect small molecules.[10] Furthermore, reported label-free measurements of small molecule interaction kinetics either are in low-throughput, nonmicroarray format[9,11−15] or indirectly measure the protein binding signal instead of the small molecules.[16] Small molecules are the most popular form of drugs,[17] and play important roles in many biological processes.[18] Therefore, a method to detect and quantify protein interactions with small molecules in a high-throughput format will have high impact on both basic research and drug discovery.

**Received:** July 3, 2014
**Accepted:** August 25, 2014
**Published:** August 25, 2014

   dx.doi.org/10.1021/ac5024556 | *Anal. Chem.* 2014, 86, 9860−9865

We have recently developed plasmonic-based electrochemical impedance microscopy (P-EIM) that can image local electrochemical impedance in real time optically with submicron spatial resolution.[19−21] P-EIM simultaneously measures both SPR[2−5] and electrochemical impedance spectroscopy (EIS)[22,23] and thus benefits from the capabilities of both techniques. Compared to traditional EIS that is based on electrical measurement, P-EIM provides imaging capability with high spatial resolution and enables high-throughput detection of microarrays. In the present work, we demonstrate P-EIM measurement of the kinetics and affinity of small molecule binding to proteins in a microarray format.

The principle of P-EIM is based on the fact that plasmon excitation at the surface of a metal film is sensitive to the surface charge of the film. When an oscillating (AC) potential is applied to the film, the SPR image intensity oscillates with the potential (Figure 1). The local image intensity is separated into

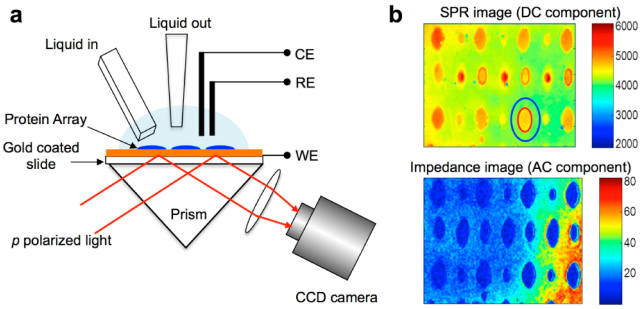


**Figure 1.** (a) Schematic illustration of P-EIM experimental setup. An AC potential modulation is applied to the gold-coated "sensor chip" (WE) via a potentiostat. A p-polarized collimated point source red LED light is directed to the sensor chip via a triangle prism at SPR resonance angle, and the reflected light is recorded via a CCD camera through a zoom lens. (b) The DC component of the image is the conventional SPR image, and the AC component is converted to admittance image via real time data processing. Images show an area on a gold sensor chip printed with proteins. The image size is 3.63 × 2.27 mm. Note that the response of each protein spot is calculated by averaging the intensity over the spot (red circle area) and then subtracting out the averaged intensity of a local referencing area (area between blue and red circles).

DC and AC components. The former gives the conventional SPR image, and the latter provides impedance or admittance (inverse of impedance) images. Compared to SPR, the impedance signal measured by P-EIM scales with the area, rather than the mass of adsorbed molecules, which is suitable for detecting small molecules.[24−26] Another important advantage of P-EIM, as shown in the present work, is that the impedance signal is insensitive to nonspecific binding and solution bulk index changes.

The present work focuses on the study of a small molecule inhibitor binding to a protein kinase, an enzyme that regulates protein activities via phosphorylation. Because phosphorylation of certain proteins promotes cancer growth, inhibiting the protein kinases can lead to treatment of these diseases. Indeed many kinase inhibitors are used as drugs, but most of them are small molecules, which are difficult to detect.[27] One example of the inhibitors studied here is imatinib (Gleevec), an FDA-approved small molecule drug for treating chronic myeloid leukemia (CML) that inhibits the enzymatic function of BCR-Abl.[28] BCR-Abl is a chimeric protein formed by the fusion of two independent genes BCR and Abl1, in which the tyrosine kinase activity of Abl1 is constantly activated. Imatinib binds to the ATP pocket of Abl1, inhibiting its activity.

## MATERIALS AND METHODS

**Materials.** Imatinib and SB202190 were purchased from BioVision Inc. (Milpitas, CA). Abl, Abl Y253F, p38-$\alpha$, and myelin basic protein (MBP) were purchased from Abcam Plc (Cambridge, MA). Carboxyl-terminated dithiol (COOH) (diSH-PEG-COOH) and hydroxy-terminated dithiol (OH) (diSH-PEG-OH) were purchased from Nanoscience Instruments, Inc. (Phoenix, AZ). All other chemicals were purchased from Sigma-Aldrich (St. Louis, MO), which were used without further purification. All buffers were prepared with deionized water.

**Sensor Chip Fabrication.** The Au sensor chips were BK-7 glass coverslips coated with 2 nm chromium and 47 nm gold by a thermal evaporator at high vacuum ($3 \times 10^{-6}$ Torr). Before surface modification, each chip was rinsed with water and ethanol and then annealed with a hydrogen flame to remove surface contamination. The cleaned chips were first immersed in ethanol solution containing 10 mM diSH-PEG-COOH and 0.5 mM diSH-PEG-OH overnight and then were thoroughly washed with water, ethanol, and water again. Next, the chips were activated with EDC/NHS protocol by coating the whole surface with a solution of 0.2 M EDC and 0.05 M NHS for 10 min and then rinsed with deionized water, dried with nitrogen gas, and immediately used for microarray printing. Protein solutions were deposited on the EDC/NHS-activated PEG-modified Au chip surfaces with a noncontact piezoelectric inkjet printer (Engineering Arts LLC) to a uniform pattern of spots with 500 mm spacing. During and after printing, precise dew-point control was used to mitigate evaporation of the printed protein spots. Relative humidity (65%) and temperature (24 °C) were precisely regulated inside the printing chamber. The sensor chips were chilled to 21 °C, which was a few degrees above the dew-point temperature (17 °C), to prevent condensation. After printing, the sensor chips were maintained with dew-point control for 50 min to allow the printed proteins to covalently bond to the sensor surface. Finally, the printed sensors were stored under argon gas at 4 °C prior to measurement.

**P-EIM Setup.** The P-EIM setup included a SPR imaging system based on the Kretschmann configuration (Figure 1a) with a temperature-controlled, point source LED (wavelength 670 nm, Hamamatsu) as light source. p-Polarized light from the LED was collimated and directed to an SF11 equilateral triangle prism (Edmund Optics) at an incident angle near SPR resonance angle. A CCD camera (Pike F-032B, Allied Vision Technologies) with a 12× variable zoom lens (Navitar) was used to record the SPR images. The Au layer on the sensor chips was used as a working electrode (WE) that was controlled with a potentiostat (Model Afcbp1, PINE Instrument Co., Grove City, PA) using Ag/AgCl as a reference electrode (RE) and a platinum wire as a counter electrode (CE). For impedance measurement, the electrode potential was modulated with an amplitude of 250 mV and a frequency of 10 Hz. The optical system was mounted on an optical bread board with an active vibration isolation system (Model Vario Basic 60, Accurion Inc., Linthicum Heights, MD).

**Flow System.** A multichannel drug perfusion system with pressure kit (SF-77B, Warner Instruments) was used to deliver sample solutions to the sensing area as showed in Figure 1a. A terminal pressure of 0.25 psi was used to maintain a constant


dx.doi.org/10.1021/ac5024556 | Anal. Chem. 2014, 86, 9860−9865

flow rate. With the flow system, the transition time between different solutions was about 1−2 s. A Flexi-Perm silicon chamber (SASTEDT, www.sarstedt.com) was placed on the top of the sensor chips to hold the solution and electrodes. A pump was used to remove the waste liquid from the chamber via plastic tubing.

**Small Molecule Sample Preparation.** Imatinib and SB202190 were first dissolved in DMSO and then were diluted to working concentration with running buffer. To avoid any matrix mismatch, the final DMSO concentration was adjusted to 0.1% (volume) in all samples and running buffer. In addition, no P-EIM response was observed upon injection of DMSO (1/500 v/v) onto sensor chips spotted with Abl or any of the control proteins.

**Data Collection and Analysis.** The time stamps of the CCD camera images and potential modulation signals were collected by a data acquisition board (NI USB-6251, National Instruments) using a custom-made Matlab program to synchronize the potential modulation with response signals. The CCD images were recorded at a speed of 378 frames per second. SPR and impedance signals of each spots were extracted from the raw images. The averaged signal from a nearby area of each spot was used to subtract out common noise and system drift (Figure 1d). Kinetic constants (association $k_a$ and dissociation $k_d$) and binding affinities ($K_D = k_d/k_a$) were calculated with a 1:1 Langmuir model by fitting the sensor response curves for each spot with a first-order kinetics.[8,29]

**Radioactive Kinase Assay.** The activity of Abl1 was tested in a radioactive kinase assay using CRK as substrate. CRK was expressed in vitro as a flag-tagged protein using Hela lysate IVTT (Thermo Scientific) and was purified by pulling down through the tag. Abl1 and CRK were incubated in the same kinase buffer used for the P-EIM assays (2.5 mM Tris-HCl and 1 mM $MgCl_2$ (pH 7.5)) supplemented with 100 $\mu$Ci/mL $^{32}$P-$\gamma$-ATP and increasing concentrations of imatinib (ranging from 0 to 1000 $\mu$M). The reaction was performed at 30 °C for 90 min. After completion of the kinase reaction, samples were loaded in a SDS-PAGE gel, and the gel was exposed to X-ray film. The bands were quantified by ImageQuantTL.

## RESULTS AND DISCUSSION

**SPR versus Impedance Signal.** Figure 2 shows the P-EIM (both SPR and impedance) results of imatinib interaction with printed Abl1 protein. Each plot is averaged SPR or impedance responses of a printed protein spot upon exposure to imatinib solution with three different concentrations, extracted from the P-EIM image sequence. Signals from area surrounding the protein spot were used as reference to subtract out common noises. As shown in Figure 2a, the SPR signals rapidly increase upon the injection of imatinib solution, followed by a slow increase phase, with the maximum increasing value scaled to the concentration of imatinib. After switching back to running buffer, SPR signals show similar two-phase responses including a rapid decrease followed by a slow decay. While the slow phases of the SPR responses reflect the real binding and dissociation signals, the rapid changes likely do not. The rapid SPR responses are not due to bulk refraction index changes because the plots are reference corrected, which subtract out the bulk index change effect. Therefore, the rapid changes must come from nonspecific absorption induced by the electrostatic attraction between positively charged imatinib and negatively charged Abl1 protein. The nonspecific absorption is weak

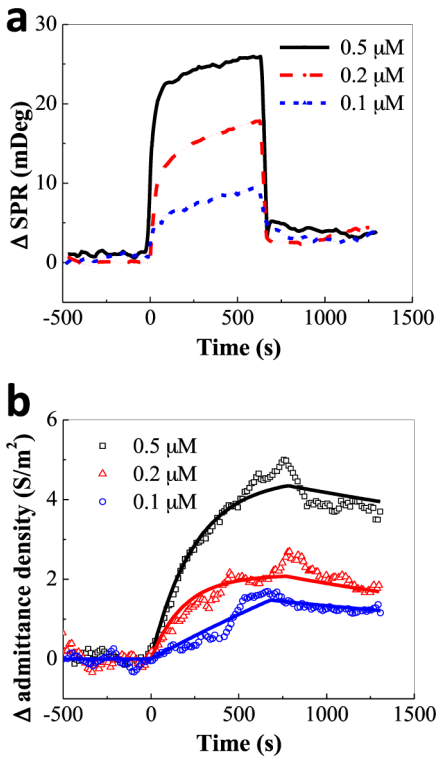


**Figure 2.** SPR (a) and admittance (b) responses to the binding of imatinib (0.1, 0.2, 0.5 $\mu$M) with Abl1 immobilized on the SPR sensor surface. The buffer contains 2.5 mM Tris-HCl and 1 mM $MgCl_2$ (pH 7.5). Solid lines in panel b are kinetic fitting curves.

compared to the specific binding between imatinib and Abl1, as it rapidly dissociated upon switching back to buffer; however, it does complicate the measurement of the binding kinetic constants.

In contrast, the simultaneously recorded impedance signals (Figure 2b) do not show any response to the nonspecific absorption. The injection of imatinib results in a single exponential increase in admittance, followed by a slow decrease after switching back to running buffer. The maximum admittance change scales with the concentration of imatinib. Global fitting of the impedance responses at different concentrations based on a 1:1 Langmuir model produces kinetic constants: $k_a = 2.2 \times 10^4$ $M^{-1}$ $s^{-1}$, $k_d = 7.4 \times 10^{-4}$ $s^{-1}$, and $K_D = 2.1 \times 10^{-8}$ M. While $k_a$ and $k_d$ are not available in literature, but $K_D$ agrees with literature reported value of $1.2 \times 10^{-8}$ M.[30,31] These results suggest that impedance can measure binding kinetics between small molecules and proteins and is immune to nonspecific adsorption.

To prove the biological relevance of these findings, the activity of Abl1 was measured by a radioactive kinase assay under exactly the same conditions used for the P-EIM experiments. We observed that Abl1 is active and is capable to phosphorylate CRK, a known substrate (Figure 3).

**Microarray Detection.** To demonstrate image-based microarray measurement, and to confirm the specificity of the impedance responses to imatinib interactions with Abl1, we have measured imatinib interaction kinetics with sensor chips spotted with different proteins. Figure 4 shows the impedance responses of imatinib interactions with different proteins, including positive (c-kit and Abl1 Y253F) and negative (p38-$\alpha$ and MBP) controls for Abl1. C-kit is another tyrosine kinase that can also be inhibited by imatinib with similar binding


dx.doi.org/10.1021/ac5024556 | Anal. Chem. 2014, 86, 9860−9865

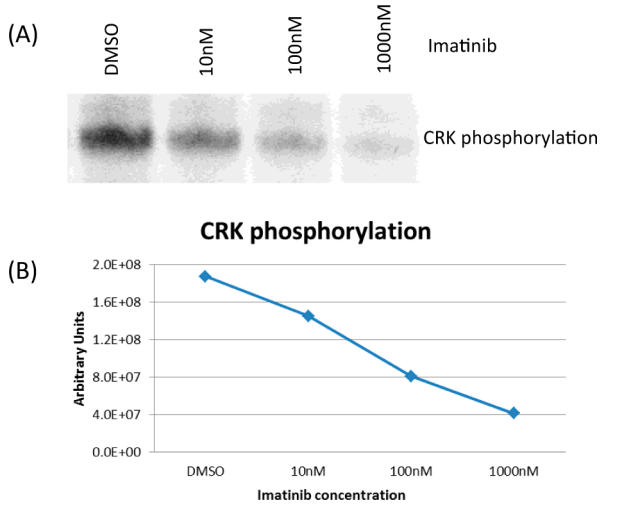


**Figure 3.** Phosphorylation of CRK by Abl1 in the presence of imatinib. The activity of Abl1 in the buffer conditions used for P-EIM experiments were tested in solution with a radioactive kinase assay. Fixed concentration of Abl1 and CRK was incubated in the presence of $^{32}$P-$\gamma$-ATP and increasing concentrations of imatinib. (A) The X-ray image shows CRK phosphorylation and (B) the data quantification.

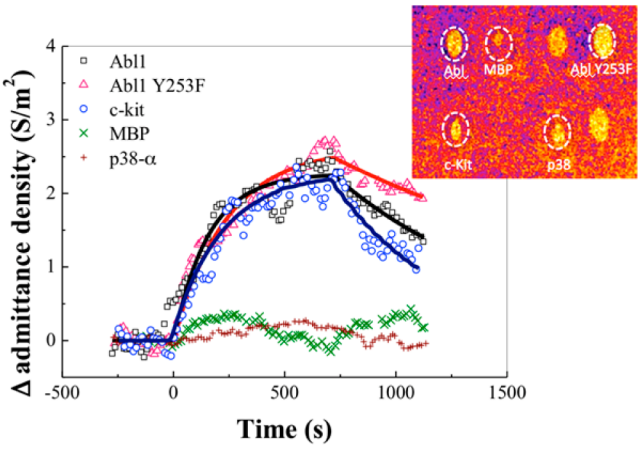


**Figure 4.** Admittance responses to the bindings of imatinib (0.2 $\mu$M) with different proteins printed on a sensor chip. The plotted values are reference corrected, as described in Figure 1. Solid lines are kinetic fitting curves. Inset: admittance amplitude image of the sensor chip shows different protein spots recorded at 600 s (circled areas).

affinity.[32] Abl1 Y253F is an Abl1 mutation found in patients that become resistant to imatinib with a slightly lower binding affinity to imatinib.[31] P38-$\alpha$ is a mitogen-activated protein kinase that does not bind to imatinib.[33] Myelin basic protein (MBP) is a nonkinase protein. Table 1 listed kinetic constants calculated from the impedance response curve of interaction between 0.2 $\mu$M imatinib and these proteins. The association

**Table 1. Interaction Kinetic Constants between Imatinib and Different Proteins**

| | $K_a$/M$^{-1}$ s$^{-1}$ | $K_d$/s$^{-1}$ | $K_D$/M | $K_D$/M (reported) |
|---|---|---|---|---|
| Abl1 | $2.2 \times 10^4$ | $7.4 \times 10^{-4}$ | $3.4 \times 10^{-8}$ | $1.2 \times 10^{-8}$ |
| Abl1 Y253F | $7.2 \times 10^3$ | $3.6 \times 10^{-4}$ | $5.1 \times 10^{-8}$ | $4.4 \times 10^{-8}$ |
| c-Kit | $2.5 \times 10^4$ | $2.7 \times 10^{-3}$ | $1.1 \times 10^{-7}$ | $1.4 \times 10^{-8}$ |
| P38-$\alpha$ | $4.7 \times 10^2$ | $1.9 \times 10^{-3}$ | $4.1 \times 10^{-6}$ | N/A |

rate constants ($k_a$), dissociation rate constants ($k_d$), and binding affinities ($K_D = k_d/k_a$) of both positive control proteins are similar to Abl1, and the binding affinities also match reported values.[34−36] Imatinib shows no meaningful binding to MBP and very weak binding to p38-$\alpha$, as we expected.

For cross-validation, we also measured another small molecule drug, SB202190, which is an inhibitor for p38-$\alpha$ but not for Abl1.[30,31] Interaction kinetics between SB202190 and several proteins are shown in Figure 5, and the calculated

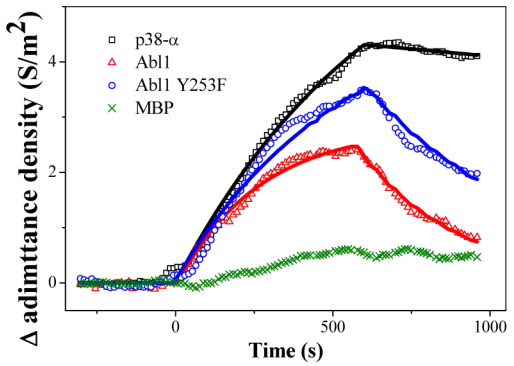


**Figure 5.** Admittance responses to the bindings of SB202190 (0.5 $\mu$M) with different proteins including Abl, Abl Y253F, MBP, and p38-$\alpha$ printed on the Au chips. Solid lines are kinetic fitting curve.

**Table 2. Interaction Kinetic Constants between SB202190 and Different Proteins**

| | $K_a$/M$^{-1}$ s$^{-1}$ | $K_d$/s$^{-1}$ | $K_D$/M |
|---|---|---|---|
| Abl1 | $6.4 \times 10^1$ | $3.5 \times 10^{-3}$ | $1.6 \times 10^{-5}$ |
| Abl1 Y253F | $5.7 \times 10^1$ | $1.8 \times 10^{-3}$ | $3.2 \times 10^{-5}$ |
| p38-$\alpha$ | $2.9 \times 10^3$ | $1.3 \times 10^{-4}$ | $4.3 \times 10^{-8}$ |

kinetic constants are shown in Table 2. The binding affinity between SB202190 and p38-$\alpha$ is $4.3 \times 10^{-8}$ M, which agrees with the reported value of $10^{-8}$ M.[30] Interestingly, SB202190 shows weak bindings with affinity larger than $10^{-5}$ M to nontarget kinases Abl1 and Abl1 Y253F, which were not discovered by the competitive binding assay.[30,31] Because these weak bindings are transient events, they are not measurable by end-point assays that rely on the measurement of equilibrium binding state. These results demonstrate the importance of kinetic measurement, which provides information on transient molecular interaction that cannot be provided by other methods. Finally, SB202190 shows negligible interactions with the negative control MBP. These results show that P-EIM is sensitive to small molecule-protein interactions and can be used for label-free, high-throughput measurement of proteins in a microarray format and can obtain quantitative molecular interaction kinetic information.

**Functional Studies.** To further demonstrate P-EIM's capability on functional studies of molecular interactions, we studied $Mg^{2+}$ dependency and competitive inhibition of imatinib binding with Abl1. There are controversial reports on the role of $Mg^{2+}$ in kinase functionality. Some studies indicate that $Mg^{2+}$ binds to the kinase surface and alters the kinase structure, which favors the binding of kinase inhibitors.[37−39] But other studies report that some kinases and inhibitors (including Abl1/imatinib) show good affinity in


dx.doi.org/10.1021/ac5024556 | Anal. Chem. 2014, 86, 9860−9865

buffers without $Mg^{2+}$ ions.[30,31] To verify the effect of $Mg^{2+}$ on imatinib/Abl1 interaction kinetics, we have studied the imatinib binding to Abl1 in buffers with and without $Mg^{2+}$. The P-EIM impedance responses (Figure 6) show clearly that the presence of $Mg^{2+}$ is critical for imatinib to bind to Abl1, because imatinib shows little binding in the magnesium-free control buffer.

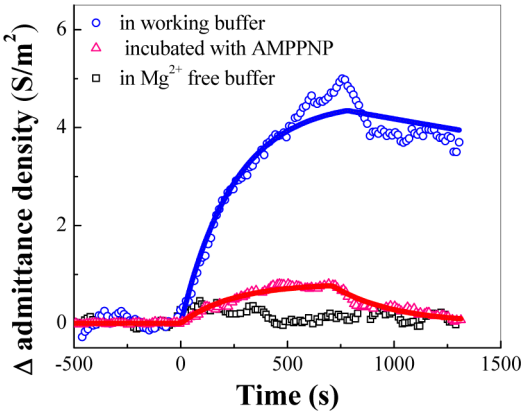


**Figure 6.** Functional study of imatinib/Abl1 interaction: effect of buffers and AMPPNP on 0.5 $\mu$M imatinib binding kinetics. Working buffer: 2.5 mM Tris buffer pH 7.5 + 1 mM $MgCl_2$; $Mg^{2+}$ free buffer: 2.5 mM Tris buffer pH 7.5 + 2 mM NaCl. For AMPPNP inhibition experiment, 100 mM AMPPNP in working buffer was used to preincubate the sensor chip for 2 h. Solid lines are kinetic fitting curve.

Imatinib inhibits the Abl1 phosphorylation function by competing with the ATP substrate at the ATP binding domain on Abl1. AMPPNP is an ATP derivative and a competitive inhibitor of most ATP-dependent systems.[33,40,41] We used AMPPNP to further validate the nature of imatinib interaction with Abl1. A sensor chip printed with Abl1 was preincubated with 100 $\mu$M AMPPNP prepared in working buffer for 2 h prior to interacting with imatinib. As shown in Figure 6, the binding of imatinib to Abl1 was mostly inhibited by AMPPNP incubation (red triangle curve). The associate rate constants dropped 1 order of magnitude to $k_a = 1.1 \times 10^3\ M^{-1}\ s^{-1}$, and the dissociate rate constants increased 1 order of magnitude to $k_d = 3.4 \times 10^{-3}\ s^{-1}$; therefore, the dissociate constants increased 2 orders of magnitude to $K_D = 3.0 \times 10^{-6}$ M. This study further confirmed that the impedance response is specific to the binding between imatinib and Abl1, and P-EIM can be used for a real-time functional study of molecular interactions.

**Limit of Detection.** In the present setup, the measured detection limit of our P-EIM setup is about 0.1 $S/m^2$ in terms of admittance (inverse of impedance, at 10 Hz, 0.25 V). Because the P-EIM signal is not directly related to the target mass, we need to make some assumptions to get a meaningful comparison with mass-based methods. The maximum binding signal from the P-EIM response curve in Figure 2b is about 5 $S/m^2$, which is 50 times larger than the detection limit. Assume the protein on the surface has a size of 5 nm and a 50% surface coverage, and the mass of the small molecule is 500 Da. Then the detection limit in term of molecular mass is about 0.3 pg/$mm^2$. Another way to quantify the sensitivity of P-EIM is to compare with the simultaneously obtained SPRi responses. As shown in Figure 2a, the maximum SPRi signal is about 5 mdeg (excluding the nonspecific binding signal) and the SPRi sensitivity of the setup is about 1 mdeg, only a 5-fold difference. Therefore, for imatinib detection, P-EIM is about 10 times more sensitive than SPRi. Because the P-EIM signal is not related to the mass of the molecule, for smaller molecules, P-EIM is more sensitive than SPR. For instance, for a 100 Da molecule, the equivalent detection limit of P-EIM is 0.06 pg/$mm^2$, 50 times more sensitive than SPRi.

**P-EIM Is Immune to Nonspecific Binding.** We have previously demonstrated that P-EIM is insensitive to bulk refractive index change and nonspecific absorption of proteins.[25] In this paper, we show that P-EIM is also insensitive to nonspecific absorption of small molecules. To explain the reason, we need to first understand the nature of the P-EIM impedance signal. The P-EIM signal is expressed in term of admittance, which measures the conductivity at the water/gold surface and is proportional to the interfacial capacitance, which is greatly affected by the molecular layer functionalized on the sensor surface.[25] At molecular scale, the P-EIM signal arises from two effects, the blocking of electrical current by the molecular binding events, which normally decrease the conductivity or admittance, and the oscillation of molecules on the surface with the potential, which depends on the charge and flexibility of the molecules.[26] Because most proteins are charged or partially charged, an electrical double layer with opposite charge will be present near the protein surface. When a periodic potential is applied to the sensor surface, the proteins on the sensor surface oscillate with the electrical field, which contributes to the measured impedance (or admittance).

Most nonspecific binding is due to weak interactions of the molecule with the surface, which contributes little to the interfacial capacitance, because the weakly bound molecules do not significantly block counterions in the solution or change the proteins immobilized on the surface. In contrast, a specific binding between a molecule and the proteins can significantly change the charge and conformation of the protein, leading to a measurable impedance response. For example, imatinib binds to an inactive conformation of Abl1 called "DFG-out" and forms an imatinib/Abl1 complex with a distinct conformation from free Abl1, which prevents the enzyme from switching to the active conformation.[42]

## ■ CONCLUSION

In summary, P-EIM can be used to detect small molecules and to measure the binding kinetics of small molecules with proteins in a microarray format. With P-EIM, both surface plasmon resonance and electrical impedance responses can be imaged simultaneously. Unlike the SPR signal, the impedance response is not scaled with the mass of analyte molecule and is insensitive to nonspecific bindings caused by electrostatic interactions. Binding kinetics and affinities between small molecule inhibitors (imatinib and SB202190) and target protein kinases (Abl1, p38-$\alpha$, and others) were obtained. The affinity results are consistent with reported literature values measured by an indirect competitive binding assay. In addition, P-EIM revealed weak interactions between SB202190 and ABL1 with $K_D > 10$ $\mu$M, which were not detectable by the indirect method. This study shows that P-EIM is an important new tool for small molecule drug discovery, biomarker validation, and disease diagnostics.

## ■ AUTHOR INFORMATION

### Corresponding Authors

*E-mail: Shaopeng.Wang@asu.edu.
*E-mail: njtao@asu.edu.
*E-mail: Joshua.Labaer@asu.edu.

**Present Address**

[⊥]State Key Laboratory of Analytical Chemistry for Life Science, School of Chemistry and Chemical Engineering, Nanjing University, Nanjing 210093, China.

**Notes**

The authors declare no competing financial interest.

## ■ ACKNOWLEDGMENTS

Financial support from NSF (no. 1151005), NIH (no. 1R44GM106579-01), and Virginia Piper foundation is acknowledged. S.W. thanks Linliang Yin and Yunze Yang at Center for Bioelectronics and Biosensors, BioDesign Institute, Arizona State University, for help on kinetic analysis.

## ■ REFERENCES

(1) Cooper, M. A. *Anal. Bioanal. Chem.* **2003**, *377*, 834−842.
(2) Homola, J. *Chem. Rev.* **2008**, *108*, 462−493.
(3) Wang, S. P.; Shan, X. N.; Patel, U.; Huang, X. P.; Lu, J.; Li, J. H.; Tao, N. J. *Proc. Natl. Acad. Sci. U. S. A.* **2010**, *107*, 16028−16032.
(4) Shan, X. N.; Foley, K. J.; Tao, N. J. *Appl. Phys. Lett.* **2008**, *92*, 3.
(5) Shan, X. N.; Huang, X. P.; Foley, K. J.; Zhang, P. M.; Chen, K. P.; Wang, S. P.; Tao, N. J. *Anal. Chem.* **2010**, *82*, 234−240.
(6) Lesuffleur, A.; Im, H.; Lindquist, N. C.; Lim, K. S.; Oh, S. H. *Opt. Express* **2008**, *16*, 219−224.
(7) Valsecchi, C.; Brolo, A. G. *Langmuir* **2013**, *29*, 5638−5649.
(8) Schasfoort, R. B. M.; Tudos, A. J. *Handbook of surface plasmon resonance*; RSC Pub.: Cambridge, UK, 2008; p 81−122.
(9) Nordin, H.; Jungnelius, M.; Karlsson, R.; Karlsson, O. P. *Anal. Biochem.* **2005**, *340*, 359−368.
(10) Inglese, J.; Johnson, R. L.; Simeonov, A.; Xia, M.; Zheng, W.; Austin, C. P.; Auld, D. S. *Nat. Chem. Biol.* **2007**, *3*, 466−479.
(11) Papalia, G. A.; Leavitt, S.; Bynum, M. A.; Katsamba, P. S.; Wilton, R.; Qiu, H.; Steukers, M.; Wang, S.; Bindu, L.; Phogat, S.; Giannetti, A. M.; Ryan, T. E.; Pudlak, V. A.; Matusiewicz, K.; Michelson, K. M.; Nowakowski, A.; Pham-Baginski, A.; Brooks, J.; Tieman, B. C.; Bruce, B. D.; Vaughn, M.; Baksh, M.; Cho, Y. H.; Wit, M. D.; Smets, A.; Vandersmissen, J.; Michiels, L.; Myszka, D. G. *Anal. Biochem.* **2006**, *359*, 94−105.
(12) Cannon, M. J.; Papalia, G. A.; Navratilova, I.; Fisher, R. J.; Roberts, L. R.; Worthy, K. M.; Stephen, A. G.; Marchesini, G. R.; Collins, E. J.; Casper, D.; Qiu, H.; Satpaev, D.; Liparoto, S. F.; Rice, D. A.; Gorshkova, I. I.; Darling, R. J.; Bennett, D. B.; Sekar, M.; Hommema, E.; Liang, A. M.; Day, E. S.; Inman, J.; Karlicek, S. M.; Ullrich, S. J.; Hodges, D.; Chu, T.; Sullivan, E.; Simpson, J.; Rafique, A.; Luginbuhl, B.; Westin, S. N.; Bynum, M.; Cachia, P.; Li, Y. J.; Kao, D.; Neurauter, A.; Wong, M.; Swanson, M.; Myszka, D. G. *Anal. Biochem.* **2004**, *330*, 98−113.
(13) Myszka, D. G. *Anal. Biochem.* **2004**, *329*, 316−323.
(14) Rich, R. L.; Day, Y. S.; Morton, T. A.; Myszka, D. G. *Anal. Biochem.* **2001**, *296*, 197−207.
(15) Zhang, M.; Peh, J.; Hergenrother, P. J.; Cunningham, B. T. *J. Am. Chem. Soc.* **2014**, *136*, 5840−5843.
(16) Kanoh, N.; Kyo, M.; Inamori, K.; Ando, A.; Asami, A.; Nakao, A.; Osada, H. *Anal. Chem.* **2006**, *78*, 2226−2230.
(17) Knox, C.; Law, V.; Jewison, T.; Liu, P.; Ly, S.; Frolkis, A.; Pon, A.; Banco, K.; Mak, C.; Neveu, V.; Djoumbou, Y.; Eisner, R.; Guo, A. C.; Wishart, D. S. *Nucleic Acids Res.* **2011**, *39*, D1035−D1041.
(18) Arkin, M. R.; Wells, J. A. *Nat. Rev. Drug Discovery* **2004**, *3*, 301−317.
(19) Wang, S. P.; Huang, X. P.; Shan, X. N.; Foley, K. J.; Tao, N. J. *Anal. Chem.* **2010**, *82*, 935−941.
(20) Shan, X.; Patel, U.; Wang, S.; Iglesias, R.; Tao, N. *Science* **2010**, *327*, 1363−1366.
(21) Foley, K. J.; Shan, X.; Tao, N. J. *Anal. Chem.* **2008**, *80*, 5146−5151.
(22) Chang, B. Y.; Park, S. M. *Annu. Rev. Anal Chem.* **2010**, *3*, 207−229.
(23) Orazem, M. E.; Tribollet, B. *Electrochemical impedance spectroscopy*; Wiley: Hoboken, N.J., 2008; p 163−182.
(24) Wang, W.; Foley, K.; Shan, X.; Wang, S.; Eaton, S.; Nagaraj, V. J.; Wiktor, P.; Patel, U.; Tao, N. *Nat. Chem.* **2011**, *3*, 249−255.
(25) Lu, J.; Wang, W.; Wang, S. P.; Shan, X. N.; Li, J. H.; Tao, N. J. *Anal. Chem.* **2012**, *84*, 327−333.
(26) MacGriff, C.; Wang, S. P.; Wiktor, P.; Wang, W.; Shan, X. N.; Tao, N. J. *Anal. Chem.* **2013**, *85*, 6682−6687.
(27) Noble, M. E.; Endicott, J. A.; Johnson, L. N. *Science* **2004**, *303*, 1800−1805.
(28) Goldman, J. M.; Melo, J. V. *Acta Haematol.* **2008**, *119*, 212−217.
(29) http://www.sprpages.nl/data-fitting/models/one-to-one.html2006, accessed September 10, 2014.
(30) Fabian, M. A.; Biggs, W. H., III; Treiber, D. K.; Atteridge, C. E.; Azimioara, M. D.; Benedetti, M. G.; Carter, T. A.; Ciceri, P.; Edeen, P. T.; Floyd, M.; Ford, J. M.; Galvin, M.; Gerlach, J. L.; Grotzfeld, R. M.; Herrgard, S.; Insko, D. E.; Insko, M. A.; Lai, A. G.; Lelias, J. M.; Mehta, S. A.; Milanov, Z. V.; Velasco, A. M.; Wodicka, L. M.; Patel, H. K.; Zarrinkar, P. P.; Lockhart, D. J. *Nat. Biotechnol.* **2005**, *23*, 329−336.
(31) Karaman, M. W.; Herrgard, S.; Treiber, D. K.; Gallant, P.; Atteridge, C. E.; Campbell, B. T.; Chan, K. W.; Ciceri, P.; Davis, M. I.; Edeen, P. T.; Faraoni, R.; Floyd, M.; Hunt, J. P.; Lockhart, D. J.; Milanov, Z. V.; Morrison, M. J.; Pallares, G.; Patel, H. K.; Pritchard, S.; Wodicka, L. M.; Zarrinkar, P. P. *Nat. Biotechnol.* **2008**, *26*, 127−132.
(32) Heinrich, M. C.; Griffith, D. J.; Druker, B. J.; Wait, C. L.; Ott, K. A.; Zigler, A. J. *Blood* **2000**, *96*, 925−932.
(33) Nemoto, S.; Xiang, J.; Huang, S.; Lin, A. *J. Biol. Chem.* **1998**, *273*, 16415−16420.
(34) Duensing, A.; Joseph, N. E.; Medeiros, F.; Smith, F.; Hornick, J. L.; Heinrich, M. C.; Corless, C. L.; Demetri, G. D.; Fletcher, C. D. M.; Fletcher, J. A. *Cancer Res.* **2004**, *64*, 5127−5131.
(35) Modugno, M.; Casale, E.; Soncini, C.; Rosettani, P.; Colombo, R.; Lupi, R.; Rusconi, L.; Fancelli, D.; Carpinelli, P.; Cameron, A. D.; Isacchi, A.; Moll, J. *Cancer Res.* **2007**, *67*, 7987−7990.
(36) Ren, A.; Y, G.; You, B.; Sun, J. *Cancer Res.* **2008**, *68*, 2266−2274.
(37) Nagar, B. *J. Nutr.* **2007**, *137*, 1518S−1523S,1548S.
(38) Marina, A.; Waldburger, C. D.; Hendrickson, W. A. *EMBO J.* **2005**, *24*, 4247−4259.
(39) Bilwes, A. M.; Quezada, C. M.; Croal, L. R.; Crane, B. R.; Simon, M. I. *Nat. Struct. Biol.* **2001**, *8*, 353−360.
(40) Yang, J.; Cron, P.; Good, V. M.; Thompson, V.; Hemmings, B. A.; Barford, D. *Nat. Struct. Biol.* **2002**, *9*, 940−944.
(41) Simanshu, D. K.; Savithri, H. S.; Murthy, M. R. *J. Mol. Biol.* **2005**, *352*, 876−892.
(42) Lin, Y. L.; Meng, Y.; Jiang, W.; Roux, B. *Proc. Natl. Acad. Sci. U. S. A.* **2013**, *110*, 1664−1669.